A synthesis of light absorption properties of the Pan-Arctic Ocean: application to semi-analytical estimates of dissolved organic carbon concentrations from space

Atsushi Matsuoka*

Affiliation 1: *Takuvik* Joint International Laboratory, Université Laval (Canada) - CNRS (France), Département de Biologie and Québec-Océan, Université Laval, Pavillon Alexandre-Vachon 1045, avenue de la Médecine, Local 2078, G1V 0A6, Canada

E-mail : Atsushi.Matsuoka@takuvik.ulaval.ca

Phone : +1 (418) 656 2131

Fax : +1 (418) 656 2339

Affiliation 2: Laboratoire d'Océanographie de Villefranche, Université Pierre et Marie Curie (Paris 6)/ Centre National de la Recherche Scientifique (CNRS), B.P. 08, Port de la Darse, Villefranche-sur-Mer Cedex, 06230, France

*Corresponding author

Marcel Babin

Affiliation 1: *Takuvik* Joint International Laboratory, Université Laval (Canada) - CNRS (France), Département de Biologie and Québec-Océan, E-mail : Marcel.Babin@takuvik.ulaval.ca

Phone : +1 (418) 656 2131

Fax : +1 (418) 656 2339

Affiliation 2: Laboratoire d'Océanographie de Villefranche, Université Pierre et Marie Curie (Paris 6)/ Centre National de la Recherche Scientifique (CNRS), B.P. 08, Port de la Darse, Villefranche-sur-Mer Cedex, 06230, France

David Doxaran

Affiliation: Laboratoire d'Océanographie de Villefranche, Université Pierre et Marie Curie (Paris

6)/ Centre National de la Recherche Scientifique (CNRS), B.P. 08, Port de la Darse, Villefranche-sur-Mer Cedex, 06230, France
E-mail : doxaran@obs-vlfr.fr
Phone : +33 (0)4 93 76 37 13
Fax : +33 (0)4 93 76 37 39

Stanford B. Hooker
Affiliation: National Aeronautics and Space Administration (NASA)/ Goddard Space Flight Center (GSFC), Code 616.2, Bldg. 28 Rm. W120D, Greenbelt, MD 20771, USA
E-mail : stanford.b.hooker@nasa.gov
Phone : +1 (301) 286 9503
Fax : +1 (301) 286 0268

B. Greg Mitchell
Affiliation : Scripps Institution of Oceanography, University of California San Diego, La Jolla, CA 92093-0238, USA
E-mail : gmitchell@ucsd.edu
Phone : +1 (858) 534 2687
Fax : +1 (858) 534 2997

Simon Bélanger
Affiliation : Université du Québec à Rimouski, Département de Biologie, Chimie et Géographie, 300 allée des Ursulines, Rimouski, Québec, G5L 3A1, Canada
E-mail : simon_belanger@uqar.qc.ca
Phone : +1 (418) 723 1986
Fax : +1 (418) 723 1849

Annick Bricaud
Affiliation: Laboratoire d'Océanographie de Villefranche, Université Pierre et Marie Curie (Paris 6)/ Centre National de la Recherche Scientifique (CNRS), B.P. 08, Port de la Darse, Villefranche-sur-Mer Cedex, 06230, France
E-mail : annick@obs-vlfr.fr
Phone : +33 (0)4 93 76 37 13
Fax : +33 (0)4 93 76 37 39

Abstract

The light absorption coefficients of particulate and dissolved materials are the main factors determining the light propagation of the visible part of the spectrum and are, thus, important for developing ocean color algorithms. While these absorption properties have recently been documented by a few studies for the Arctic Ocean [e.g., Matsuoka et al., 2007, 2011; Ben Mustapha et al., 2012], the datasets used in the literature were sparse and individually insufficient to draw a general view of the basin-wide spatial and temporal variations in absorption. To achieve such a task, we built a large absorption database at the pan-Arctic scale by pooling the majority of published datasets and merging new datasets. Our results show that the total non-water absorption coefficients measured in the Eastern Arctic Ocean (EAO; Siberian side) are significantly higher than in the Western Arctic Ocean (WAO; North American side). This higher absorption is explained by higher concentration of colored dissolved organic matter (CDOM) in watersheds on the Siberian side, which contains a large amount of dissolved organic carbon (DOC) compared to waters off North America. In contrast, the relationship between the phytoplankton absorption ($a_\varphi(\lambda)$) and chlorophyll *a* (chl *a*) concentration in the EAO was not significantly different from that in the WAO. Because our semi-analytical CDOM absorption algorithm is based on chl *a*-specific $a_\varphi(\lambda)$ values [Matsuoka et al., 2013], this result indirectly suggests that CDOM absorption can be appropriately derived not only for the WAO but also for the EAO using ocean color data. Derived CDOM absorption values were reasonable compared to *in situ* measurements. By combining this algorithm with empirical DOC versus CDOM relationships, a semi-analytical algorithm for estimating DOC concentrations for coastal waters at the Pan-Arctic scale is presented and applied to satellite ocean color data.

Antonio 12/11/13 2:18 PM
Deleted: ed

1. Introduction

The Arctic Ocean faces dramatic changes in physical environments driven by ongoing global warming. Decreases in both sea ice extent and thickness [Comiso et al., 2008; Kwok, 2007; Stroeve et al., 2008] facilitates the propagation of light into the water column, creating favorable conditions for phytoplankton photosynthetic processes when nutrients are available in the upper layer of the water column [e.g., Ardyna et al., 2013]. Recent papers showed that an increase in primary production (PP) is significantly and positively correlated with open water area [Arrigo and van Dijken, 2011], suggesting that autochthonous dissolved organic carbon (DOC) resulting from the increased PP could be a non-negligible source for open waters [Wheeler et al., 1996]. More importantly, in terms of the DOC budget, DOC concentrations in coastal waters are much higher than for open waters [Benner et al., 2005; Stedmon et al., 2011; Amon et al., 2012, Matsuoka et al., 2012]. In addition to autotrophic sources, it is expected that recent increases in river discharges modify [Stedmon et al., 2011]: 1) the total amount of DOC discharged to the Arctic Ocean, 2) the seasonality of the riverine export by increasing the flux of DOC during the base flow period (November to May), when material is older, more bio-refractory and could be transported far in the Arctic Ocean under the ice cover in winter, 3) the relative contribution of the large Arctic rivers (e.g., Lena vs. Yenisei) with consequences on DOC distribution in the Arctic Ocean. However, a comprehensive method for quantifying and continuously monitoring DOC concentrations, which takes into account their temporal and geographical variability at the Pan-Arctic scale, is presently not available.

One of the best approaches to achieve this task is to apply a semi-analytical algorithm to satellite ocean color data. Such an algorithm was recently developed for southern Beaufort Sea (Mackenzie Shelf area) waters in the Canadian Arctic [Matsuoka et al., 2013]. The accuracy in the estimates of DOC concentrations using this approach relies upon an accurate retrieval of absorption coefficients of colored dissolved organic matter, CDOM at 443 nm ($a_{CDOM}(443)$, m^{-1}), and on the robustness of the relationship between DOC and $a_{CDOM}(443)$. The CDOM algorithm of Matsuoka et

al.[2013] is based on a parameterization of absorption properties. To determine whether this algorithm can be applied to regions of the Arctic Ocean other than the Mackenzie Shelf area, the geographical variability of those optical properties must be determined.

The main objective of the present study is therefore to examine absorption properties at the Pan-Arctic scale. Based on these results, a semi-analytical algorithm for estimating DOC concentrations in coastal waters at the Pan-Arctic scale is presented and applied to satellite ocean color data.

2. Datasets and methods

2.1. *In situ* measurements

To provide a general overview of absorption properties, we built a large absorption database at the Pan-Arctic scale by pooling the majority of published data (Figure 1; Table 1). In the Western Arctic Ocean (WAO), data were collected during the following five cruises during spring to autumn: the Western Arctic Shelf Basin Interaction, SBI 1) spring and 2) summer cruises aboard the *USCGS Healy* (referred to as SBI spr: 5 May to 15 June 2002, and SBI sum: 16 July to 26 August 2002, respectively), 3) the Japanese Arctic cruise aboard *R/V Mirai* (referred to as MR: 1 September to 13 October 2004), 4) the Canadian Arctic Shelf Exchange Study (CASES) cruise aboard *CCGS Amundsen* (referred to as CASES: 16 May to 2 August 2004), and 5) the MALINA cruise aboard *CCGS Amundsen* (referred to as MALINA: 30 July to 27 August 2009). In the Eastern Arctic Ocean (EAO), data were collected during the NABOS cruise aboard *R/V Viktor Buynitsky* (referred to as NABOS: 14 September to 30 September 2007). To minimize geographic bias due to a large number of data in the Chukchi and western part of the southern Beaufort Seas, absorption datasets from ICESCAPE2010 and ICECAPE2011 cruises (referred to as ICESCAPE1: 15 June to 22 July 2010, and ICESCAPE2: 25 June to 29 July, 2011, respectively) were not used for our main results. Instead, these independent datasets were used for evaluating the Bricaud and Stramski [1990] method (see Appendix A2). Radiometric data obtained from MALINA, ICESCAPE1, and ICESCAPE2 were used for evaluating a semi-analytical CDOM algorithm

Antonio 12/11/13 3:02 PM
Comment [1]: Need to mention what was being evaluated here – aph.

developed by Matsuoka et al.[2013] (see sections 2.2 to 2.4 for details).

Discrete water samples were collected using Niskin bottles, except at the surface where a clean container was used during the MR cruise. During the six cruises, 30, 29, 51, 94, 37, and 57 stations (SBI spr, SBI sum, MR, CASES, MALINA, and NABOS, respectively) were visited to collect water samples for pigment and absorption analyses within the euphotic zone (i.e., between the surface and the euphotic depth, z_{eu}, defined as the depth of penetration of 1% of the surface photosynthetically available radiation (PAR)). Absorption coefficients of particles ($a_p(\lambda)$, m^{-1}) retained on GF/F filters were determined from 350 to 750 nm using a MPS-2400 spectrophotometer (Shimazu Corp.) for SBI spr, SBI sum, and MR, and a Lambda 19 (Perkin-Elmer) for CASES, NABOS, and MALINA. Because two spectrophotometers with different geometries were used for absorption measurements, the corresponding and appropriate pathlength amplification effect caused by highly scattering GF/F filter, known as the β-factor [Mitchell and Kiefer, 1988], was taken into account for each instrument (see Table 1 for details).

Phytoplankton pigments retained on the filters were extracted using methanol [Kishino et al., 1985]. Absorption coefficients of non-algal particles, NAP ($a_{NAP}(\lambda)$, m^{-1}) were determined on the de-pigmented filter. Phytoplankton absorption coefficients ($a_\varphi(\lambda)$, m^{-1}) were finally obtained by subtracting $a_{NAP}(\lambda)$ from $a_p(\lambda)$. For the NABOS cruise, only $a_p(\lambda)$ data were available. To obtain $a_\varphi(\lambda)$ and $a_{NAP}(\lambda)$, a numerical decomposition method proposed by Bricaud and Stramski [1990] was applied to this dataset. An evaluation of this method for Arctic samples is presented in Appendix A2. All absorption measurements were made following the NASA Ocean Optics Protocols [Mitchell et al., 2003] except MALINA data, for which we followed Rottgers and Gehnke [2012]. Spectral slopes of NAP, S_{NAP} (nm^{-1}) were calculated by fitting a nonlinear model to the data from 380 to 730 nm, excluding the 400-480 and 620-710 nm ranges to avoid any residual pigment absorption [Babin et al., 2003].

For the CDOM absorption measurements, water samples were filtered using 0.2 µm pore-size filters immediately after sampling [see details for sample preparation in Mitchell et al., 2003 and

Antonio 12/11/13 3:00 PM
Deleted: bleached

168 Matsuoka et al., 2012]. Absorption coefficients of CDOM ($a_{CDOM}(\lambda)$, m^{-1}) were determined from
169 280 to 700 nm using a MPS2400 spectrophotometer (Shimazu corp.) for SBI spr, SBI sum, and
170 MR. For CASES cruise, the filtrates were frozen at -20 °C and shipped to the laboratory at
171 Rimouski. $a_{CDOM}(\lambda)$ spectra were then measured using a Lambda 35 (Perkin-Elmer) from 250 to
172 800 nm. Both spectrophotometers were equipped with 10 cm quartz cells [Bélanger et al., 2006;
173 Matsuoka et al., 2011]. For the MALINA cruise, an UltraPath liquid waveguide system was used
174 (World Precision Instruments, Inc.), and $a_{CDOM}(\lambda)$ was obtained from 200 to 735 nm [Matsuoka et
175 al, 2012]. For the NABOS cruise, $a_{CDOM}(\lambda)$ was obtained at 412, 443, 488, 510, 532, 555, 630, 676,
176 and 715 nm using a ac-9 (WETLabs) with 0.2 µm inlet-filter [Pegau et al., 2003]. Spectral slopes of
177 CDOM absorption (S_{CDOM}, nm^{-1}) were calculated by fitting a nonlinear model to the data from 350
178 to 500 nm, except for the NABOS cruise, for which S_{CDOM} was calculated using $a_{CDOM}(\lambda)$ at 412,
179 440, 488, and 510 nm. The total non-water absorption coefficient, $a_{tw}(\lambda)$ was calculated as the sum
180 of $a_{\varphi}(\lambda)$, $a_{NAP}(\lambda)$, and $a_{CDOM}(\lambda)$.

181 Chl *a* concentrations were determined using either fluorometric methods [chl a^{fluo}: Holm-
182 Hansen et al., 1965; Suzuki and Ishimaru, 1990], high performance liquid chromatography (HPLC)
183 [chl a^{HPLC}: Ras et al., 2008], or both. Comparison between chl a^{fluo} and chl a^{HPLC} showed
184 reasonable agreement (r^2 = 0.89, intercept = 0.11, slope = 0.98, N = 177; see Appendix A1). In this
185 study, chl a^{HPLC} was used if available. Otherwise, chl a^{fluo} was used.

186 The detailed method for measuring concentrations of suspended particulate matter (SPM) is
187 documented in Doxaran et al. [2012]. Briefly, 0.2 to 6 L of seawater was filtered on a pre-
188 combusted and pre-weighted GF/F filter. After filtration of seawater, filters were systematically
189 rinsed with 0.2 to 0.6 L of Milli-Q water to remove sea salt. The reason for rinsing using Milli-Q
190 water instead of ammonium formate solution proposed by ICES [2004] is that the latter product
191 may leave carbon deposits on the filters. This would have contaminated the CHN analyses, also
192 made on the SPM filters to determine their particulate carbon content [see Doxaran et al., 2012].
193 Concentration of SPM was then calculated as the difference in weight before and after filtration

Antonio 12/11/13 3:08 PM
Comment [2]: Why not simply use the sums of ap and acdom? This would avoid any uncertainties from the de-pigmentation and the spectral decomposition for the NABOS cruise.

194 divided by the volume of the sample (in g m^{-3}). The SPM concentrations were measured for CASE,
195 NABOS, and MALINA cruises.
196
197 2.2. Calculation of remote sensing reflectance
198 In-water upwelled radiance (L_u, μW cm^{-2} nm^{-1} sr^{-1}) and downward irradiance (E_d, μW cm^{-2} nm^{-1})
199 were obtained at 19 wavelengths spanning from 320 to 780 nm following the NASA Ocean
200 Optics Protocols [Mueller and Austin, 1995] and Hooker et al. [2013]. Briefly, a compact-optical
201 profiling system (C-OPS, Biospherical Instruments Inc.) [Morrow et al. 2010] was deployed at 36
202 and 19 stations for MALINA and ICESCAPE1 cruises, respectively. For the ICESCAPE2 cruise, a
203 profiling reflectance radiometer series 800 (PRR-800, Biospherical Instruments Inc.) was deployed
204 at 24 stations. In the present study, the independent datasets from these cruises were used to
205 evaluate our semi-analytical algorithm for deriving CDOM absorption developed by Matsuoka et
206 al.[2013]. The above-water global solar irradiance (E_s) measurements were used to correct the E_d
207 and L_u data for change in the incident light field during water column profiling. The in-water
208 measurements were made far away from the main ship body to minimize platform pertubations, and
209 the above-water solar irradiance measurements were made to avoid superstructure shadows and
210 reflections. The tilt angles were always less than 5°, as recommended by the NASA Ocean Optics
211 Protocols [Mueller and Austin, 1995]. Subsurface L_u at null depth (i.e., $L_u(0^-, \lambda)$) were obtained
212 from the slope and intercept given by the least-squares linear regression of the log-transformed
213 upwelled radiance versus *z*. The principal data product used here is the remote sensing reflectance,
214 $R_{rs}(\lambda) = 0.54\, L_u\,(0^-, \lambda)/\, E_s\,(\lambda)$, where λ indicates wavelength. In this study, $R_{rs}(\lambda)$ at six wavelengths
215 (i.e, 412, 443, 490, 532, 555, and 670 nm corresponding approximately to Moderate-Resolution
216 Imaging Spectroradiometer, MODIS ocean color bands) were used to derive $a_{CDOM}(\lambda)$ at 443 nm
217 values based on a method explained in section 2.4 [Matsuoka et al., 2013].
218
219 2.3. Ocean color data

Monthly averaged climatology data over the 2002 to 2012 period for $R_{rs}(\lambda)$ at 412, 443, 488, 531, 555, and 670 nm, obtained from the MODIS Aqua ocean color sensor (http://oceandata.sci.gsfc.nasa.gov/MODISA/Binned/Monthly_Climatology/), were used in this study. A semi-analytical algorithm for deriving $a_{CDOM}(443)$ based on the method detailed in section 2.4 [Matsuoka et al., 2013] was then applied to the $R_{rs}(\lambda)$ data. DOC concentrations in coastal waters were estimated using the relationships between DOC and $a_{CDOM}(443)$ as shown in section 2.4.

2.4. Semi-analytical algorithms for deriving CDOM absorption and DOC concentration

A detailed description of our semi-analytical CDOM absorption algorithm is given in Matsuoka et al. [2013]. Briefly, this algorithm produces $a_{CDOM}(443)$ using $R_{rs}(\lambda)$ at six wavelengths in the visible spectral domain corresponding to ocean color sensors (e.g., MODIS and MEdium Resolution Imaging Spectrometer, MERIS) by minimizing the difference between measured $R_{rs}(\lambda)$ and $R_{rs}(\lambda)$ calculated using absorption and backscattering coefficients, as in the Garver-Siegel-Maritorena (GSM) algorithm [Garver and Siegel, 1997; Maritorena et a., 2002]. The following modifications were included: 1) chl *a*-specific absorption coefficients of phytoplankton for Arctic waters [Matsuoka et al., 2011] were used; 2) spectral slopes of CDM absorption, S_{CDM} (nm^{-1}) and of backscattering of particles ($b_{bp}(\lambda)$, m^{-1}), η (dimensionless) were set either to be constants or as functions of $R_{rs}(\lambda)$ (those parameters were determined based on a sensitivity analysis following Matsuoka et al.[2013]; 3) $b_{bp}(555)$ was calculated using $b_{bp}(443)$ and η; 4) $a_{NAP}(443)$ was calculated using the empirical relationship between $a_{NAP}(443)$ and $b_{bp}(555)$ obtained for Arctic waters [i.e., $a_{NAP}(443) = b_{bp}(555)/0.2393$; Matsuoka et al., 2007]; and 5) $a_{CDOM}(443)$ was obtained by subtracting $a_{NAP}(443)$ from $a_{CDM}(443)$. To estimate DOC concentrations in the near-surface coastal waters using ocean color data, a relationship between DOC and $a_{CDOM}(\lambda)$ needs to be established. Walker et al. [in press] recently showed a consistent relationship between DOC and CDOM absorption coefficient at 350 nm [$a_{CDOM}(350)$, m^{-1}] for waters at the mouth of the five major Arctic

rivers (i.e., Lena, Yenisei, Ob, Mackenzie and Kolyma rivers; DOC = 245 + 171 * $a_{CDOM}(443)$). The latter DOC vs. $a_{CDOM}(443)$ relationship was obtained by assuming a S_{CDOM} of 0.0175 nm^{-1} calculated using data from 350 to 600 nm in the EAO, as reported by Aas et al.. 2002, to convert $a_{CDOM}(350)$ to $a_{CDOM}(443)$. Stedmon et al.[2011] reported a lower S_{CDOM} (0.0167 nm^{-1}) using the data from 300 to 650 nm. While the use of a different data range for calculating a spectral slope makes it difficult to compare results [Twardowski et al., 2004], the spectral slope reported by Stedmon et al.[2011] would not be significantly different from the one by Aas et al. [2002] if the same data range is used. In any case, the choice of a spectral slope resulted in a change of only 7 % for the slope of the DOC versus $a_{CDOM}(443)$ relationship, which did not influence our results.

In the relationship converted in this study (DOC = 245 + 171 * $a_{CDOM}(443)$), the intercept is too high for the mouth of the Mackenzie river (245 µM) in the WAO, when compared to published values (55-97 µM: Osburn et al., 2009; Matsuoka et al., 2012). The high intercept may be due to a lower DOC to $a_{CDOM}(443)$ ratio at high $a_{CDOM}(443)$ values (> 1.1 m^{-1}) in the EAO (see also Figure 10). Thus, for the WAO, we used the relationship recently obtained by Matsuoka et al. [2012] (i.e., DOC (µM) = 55 + 357 * $a_{CDOM}(443)$). These two regressions were used to estimate DOC concentrations from space using $a_{CDOM}(443)$ derived from ocean color data.

2.5. Statistical analyses

Bio-optical quantities are often log-normally distributed in natural environments [Campbell, 1995]. The normality of distribution for chl *a*, $a_{\varphi}(\lambda)$, $a_{CDOM}(\lambda)$ and $a_{NAP}(\lambda)$ values was verified for Arctic waters using a Kolmogorov-Smirnov test [Matsuoka et al., 2011]. Geometric mean and geometric SD were thus obtained for these variables in this study. Otherwise, arithmetic mean and SD were used.

3. Results and discussion

3.1. Absorption budget

Antonio 12/11/13 8:35 PM
Comment [3]: Don't understand why this equation is included in this sentence. The topic is DOC to aCDOM350 not aCDOM443. Is this equation from Walker et al.? If the article is in press, then the citation in the reference list should include the journal name.

Antonio 12/11/13 8:39 PM
Comment [4]: This sentence does not make sense as written. How does one apply S to obtain DOC vs aCDOM443 relationship. Was S used to compute aCDOM443 from aCDOM350? What was the reference wavelength used if the widely used spectral slope equation was applied?

Antonio 12/11/13 8:43 PM
Comment [5]: One point that should be made is whether aCDOM443 is retrieved equally well from the S300 or the S350 slopes. A more significant point is how variable is S for the various systems? One of the problems here is that two different parameters are being compared S350 and S300. How do the different S parameters impact aCDOM443? Comparing the difference in slope of DOC vs aCDOM443 seems less of an issue. Fundamentally, it's the differences in aCDOM443 between the 2 S paramters that matter.

Antonio 12/11/13 8:52 PM
Comment [6]: Clearly, the DOM composition differs between the EAO and Mackenzie River resulting in the different DOC to CDOM ratios. This is not unusual. There are likely differences in vegetation between the watersheds that influence the relative amounts of chromophoric and non-chromophoric DOM.

Antonio 12/11/13 8:59 PM
Comment [7]: Did you test the normality of the log values for these variables or the non-transformed values?

In view of ocean color applications at the pan-Arctic scale, the total non-water absorption properties were examined first. We found that $a_{tw}(443)$ in coastal waters (i.e., CASES, NABOS, and MALINA) tended to be higher than in oceanic waters (i.e., SBI spr, SBI sum, and MR) (Figure 2). This result is consistent with the fact that river discharge largely influences absorption properties for the southern Beaufort and Siberian Seas, but not for the Chukchi Sea and the western part of the Beaufort Sea [Matsuoka et al., 2011, 2012; Amon et al., 2012]. Over the Siberian shelves (or EAO), $a_{tw}(443)$ was significantly higher ($p < 0.001$) than in the southern Beaufort Sea (or WAO) (Figure 2; Table 1), which was also indirectly shown by Aas et al.[2002] using spectral diffuse attenuation coefficients of downwelling irradiance, ($K_d(\lambda)$, m^{-1}) (the total non-water absorption was not directly measured in their work).

The higher $a_{CDOM}(443)$ of the EAO was partly responsible for the higher $a_{tw}(443)$ compared to WAO (relative contribution to $a_{tw}(443)$ of 85 ± 7 % and 67 ± 19 %, respectively; Table 1 and Figure 3). This is also consistent with the fact that the load of DOC and CDOM in the Siberian rivers (e.g., Lena, Yenisei, and Ob) is significantly higher than the Mackenzie river [Stedmon et al., 2011]. CDOM absorption is strongly correlated with DOC concentrations in coastal waters of the Arctic Ocean [Matsuoka et al., 2012; Walker et al., in press]. The higher CDOM absorption in the EAO likely reflects higher DOC concentrations in high latitude watersheds of Siberia compared to those in North America [Raymond et al., 2007]. This topic is further discussed in the section 3.4.

The strong contribution of CDOM absorption is consistent with the fact that the Arctic Ocean receives the largest amount of freshwater relative to its volume [11 % of global freshwater input while its volume is only 1 % of the global ocean, Siklomanov, 1993]. While this high contribution of CDOM absorption is well acknowledged especially for the WAO in both coastal and offshore waters [Bélanger et al., 2006, 2013; Matsuoka et al., 2007, 2009, 2011], it is evidenced as well here for the EAO (Figure 4), confirming the characteristic for the whole Arctic region (68 ± 19 %, N = 603; Table 1). Consequently, waters include high proportion of CDOM for both oceanic and coastal waters at the Pan-Arctic scale, significantly influencing several estimates such as $K_d(\lambda)$ and primary

298 production (PP) as derived from ocean color data [Reynolds et al., 2013; Arrigo et al., 2013].

299

300 3.2. Parameterization

301 While Matsuoka et al.[2011] examined absorption properties of the WAO, the majority of the
302 data in that study were obtained for oceanic waters. To generalize the absorption properties for
303 Arctic waters, large datasets of absorption in coastal waters from both the southern Beaufort and
304 Siberian Seas were added and analyzed in this study.

305 To examine differences in bio-optical properties between WAO and EAO, $a_p(443)$ was plotted
306 as a function of chl *a* (Figure 5a). Even when the outliers, observed outside the 95 % confidence
307 intervals, were included, $a_p(443)$ showed significant positive correlation with chl *a* ($r^2 = 0.62$, $p <$
308 0.0001; $N = 657$), which was quite similar to the correlation observed by Bricaud et al. [1998] at
309 lower latitudes. High pigment packaging effect has been acknowledged as a common feature for
310 Arctic phytoplankton absorption, resulting in lower chl *a*-specific $a_\varphi(\lambda)$ ($a^*_\varphi(\lambda)$, m^2 mg chl a^{-1})
311 values relative to those at lower latitudes [e.g., Mitchell, 1992; Matsuoka et al., 2011]. Because
312 particulate absorption is composed of phytoplankton and NAP absorption, higher NAP absorption
313 values for Arctic waters compared to those at lower latitudes ($p < 0.05$; Table 2) leads to a similar
314 $a_p(443)$ versus chl *a* relationship. The higher NAP likely originates from materials derived from
315 glaciers and delivered by river runoff or from coastal erosion by ice [Mitchell and Holm-Hansen,
316 1991; Hodgkins et al., 2003], by accumulation of organic material in sea ice due to atmospheric
317 deposition of aerosols or by ice algae *in situ* production [Bélanger et al., 2013].

318 Figure 5b represents the relationship between $a_\varphi(443)$ and chl *a*. Less variability in this
319 relationship was observed compared to the $a_p(443)$ versus chl *a* relationship. A strong correlation
320 between the two variables was found ($r^2 = 0.78$, $p < 0.0001$; $N = 657$). As expected, this regression
321 line at chl $a < 1.0$ mg m^{-3} was significantly below the one obtained by Bricaud et al. [1998] at lower
322 latitudes, demonstrating the higher pigment packaging effect for Arctic waters.

323 It should be stressed that while significantly higher $a_{CDOM}(443)$ in the EAO was observed

compared to WAO (Figures 3 and 4), the $a_\varphi(443)$ versus chl *a* relationships between the EAO (or NABOS dataset) and WAO (or the rest of the datasets) showed no significant difference or were statistically similar (p = 0.35, F-test). Despite the geographical difference between the WAO and EAO, this result suggests that the same relationship can be applied for both. More importantly, because our semi-analytical CDOM absorption algorithm is based on chl *a*-specific $a_\varphi(\lambda)$ estimates [Matsuoka et al., 2013], this result highlights that our algorithm can be applied not only for WAO but also for EAO.

Antonio 12/11/13 9:18 PM
Comment [8]: The log-log plot in Fig. 5b shows quite a bit of scatter around the regression line that would likely yield quite high uncertainty in satellite retrievals.

Matsuoka et al.[2011] and Wang et al.[2005] showed that $a_\varphi(\lambda)$ in the visible spectral domain is highly correlated with $a_\varphi(443)$ which can be obtained using ocean color data. While a large dataset including both oceanic and coastal waters was used in this study (N = 993), $a_\varphi(\lambda)$ showed excellent correlation with $a_\varphi(443)$ (Figure 6 and Table 3). This kind of statistical approach allows obtaining spectral $a_\varphi(\lambda)$ values using ocean color data, which can be further used for operating a spectral primary production model from space.

Statistics for $a_{CDOM}(443)$ and $a_{NAP}(443)$ and their spectral slopes are shown in Table 4. Results are consistent with those provided by Matsuoka et al. [2011], although much larger datasets obtained from various locations were used in the present study (N = 859, compared to N = 408 in Matsuoka et al., 2011), suggesting the ubiquitous features in waters at the Pan-Arctic Ocean.

3.3. Evaluation of the CDOM absorption algorithm

Estimates of DOC concentrations in Arctic coastal waters using ocean color data are reliable when CDOM absorption values are appropriately derived [Matsuoka et al., 2013]. We evaluated the performance of a tuned semi-analytical CDOM absorption algorithm using our Arctic datasets (Figure 7); in this study, all data from MALINA, ICESCAPE1 and ICESCAPE2 datasets were used for this evaluation, whereas Matsuoka et al. [2013] only used data from the MALINA dataset. It is important to recall that this evaluation was performed using independent datasets (e.g., MALINA, ICESCAPE1, and ICESCAPE2 datasets) that were not used for developing the algorithm (i.e., data

from SBI spr, SBI sum, and MR cruises were used for this development). Results showed that the semi-analytical CDOM algorithm works reasonably well with sufficient accuracy (Table 5). On average, $a_{CDOM}(443)$ can be derived using our CDOM algorithm within 9 %. Only four data points were located above the 50 % error intervals (circles in Figure7). The $a_{CDOM}(443)$ estimates at these points were likely influenced by the presence of mycosporine-like amino acids (MAAs) which were apparent in $a_{\varphi}(\lambda)$ spectra (see Appendix A3). Although *in situ* $R_{rs}(\lambda)$ data in the EAO are currently not available, this result gives confidence that $a_{CDOM}(443)$ can be derived accurately using ocean color data.

Antonio 12/11/13 9:44 PM

Comment [9]: This 9% values is not consistent with the data shown on Fig. 7. There are many data points close to +/-35% error compared to points that fall on the 1:1 line. What is the mean absolute percent difference of the error values plotted on Fig. 7?

3.4. Ocean color application

Based on the evaluation of our CDOM algorithm as well as bio-optical properties as shown above, we derived $a_{CDOM}(443)$ from satellite data ($a^{sat}_{CDOM}(443)$, m^{-1}) by applying this algorithm to MODIS climatological data (Figure 8). To our knowledge, this is the first synoptic view of $a_{CDOM}(443)$ for the whole Arctic Ocean using a semi-analytical approach. Waters with high CDOM absorption are more widely distributed in the EAO (e.g., Laptev and Kara Seas) than in the WAO (e.g., southern Beaufort Sea). For August, geometric mean (G. Mean) and geometric standard deviation (G. SD) values of $a^{sat}_{CDOM}(443)$ in the southern Beaufort Sea (0.059 and 2.363 m^{-1}, respectively) were similar to our field observations for the MALINA cruise (0.055 and 2.265 m^{-1}, respectively) during the same time period [Matsuoka et al., 2012]. G. Mean and G. SD values for $a^{sat}_{CDOM}(443)$ in the Laptev (0.138 and 2.833 m^{-1}, respectively) and Kara Seas (0.073 and 3.037 m^{-1}, respectively) are higher than those in the southern Beaufort Sea (Figure 9). The highest $a^{sat}_{CDOM}(443)$ value observed in the Kara Sea (4.353 m^{-1}) is consistent with *in situ* measurements [up to 5 m^{-1}; Aas et al., 2002; Heim et al., 2013; Orek et al., 2013, Walker et al., in press]. In addition to our evaluation shown in Figure 7, this result highlights the reliability of satellite ocean color data for Arctic waters [see also Figure 5 in Matsuoka et al., 2013].

To estimate DOC concentrations in coastal waters using ocean color data, a DOC concentration

versus CDOM absorption relationship needs to be established. Matsuoka et al. [2012] recently showed a strong correlation between the two variables in southern Beaufort Sea waters ($r^2 = 0.97$; $p < 0.0001$). Similarly, DOC concentrations were well correlated with $a_{CDOM}(443)$ in the EAO [Walker et al., in press]. It is important to note that the DOC versus $a_{CDOM}(443)$ relationships differ between the WAO and EAO (Figure 10), suggesting that different relationships between DOC and $a_{CDOM}(443)$ need to be applied for EAO and WAO.

To estimate DOC concentrations in the near surface waters of the Arctic Ocean, the regression of DOC versus $a_{CDOM}(443)$ shown in Figure 10 was applied to $a^{sat}_{CDOM}(443)$ image. Similarly to $a^{sat}_{CDOM}(443)$ distribution, waters showing high DOC concentrations were widely distributed in the EAO compared to WAO (Figure 11). The G. means of DOC concentrations estimated from satellite data (DOC^{sat}, µM) in the southern Beaufort Sea (82 µM) were of the same order of magnitude as *in situ* measurements for the MALINA cruise [79 µM: Matsuoka et al., 2012]. The values in the Laptev (279 µM) and Kara Seas (267 µM) were higher than in the southern Beaufort Sea (Figure 12), which is consistent with *in situ* measurements [Amon et al., 2012; Walker et al., in press]. The high DOC concentrations in the EAO are likely due to higher DOC concentrations in the high latitude watersheds of Siberia compared to those in North America [Raymond et al., 2007; Stedmon et al., 2011]. Ongoing global warming will likely increase the release of presently sequestered carbon that originates, in part, from thawing of the permafrost [e.g., Frey and Smith, 2005; Stedmon et al., 2011]. Continuous monitoring and quantification of DOC concentrations and the budget for the whole Arctic Ocean are therefore urgently required to better understand modifications in carbon cycling as a result of global warming.

Antonio 12/12/13 9:35 AM
Comment [10]: What about a statistical evaluation of satellite-derived DOC and in situ DOC?

Conclusions

This study examined light absorption properties in the Pan-Arctic Ocean using a large dataset including both oceanic and coastal waters. Our results clearly showed the specificity of those properties: high proportion of CDOM absorption, high pigment packaging effect. Despite the high

proportion of CDOM absorption to the total non-water absorption, the relationship between phytoplankton absorption at 443 nm and chl *a* concentration was not significantly different between the WAO and EAO. Our semi-analytical CDOM algorithm depends on chl *a*-specific $a_{\varphi}(\lambda)$ estimates, highlighting the applicability for the whole Arctic Ocean. Using DOC versus $a_{CDOM}(443)$ relationships, DOC concentrations in coastal waters can now be estimated semi-analytically using satellite ocean color data. Our statistical results demonstrated that both $a_{CDOM}(443)$ values and DOC concentrations obtained using satellite ocean color data are reasonable compared to *in situ* measurements, suggesting its potential utility for obtaining a quantitative estimate of the carbon budget of the Arctic Ocean.

The DOC budget of the Arctic Ocean is expected to change rapidly due to sea ice reduction, permafrost thawing, and river discharge increases as consequences of global warming. To examine this issue temporally and geographically using satellite ocean color data, we developed a semi-analytical algorithm for estimating DOC concentrations in Arctic coastal waters. Compared to empirical algorithms that have been proposed [e.g., Mannino et al., 2008; Fichot and Benner, 2011], because CDOM absorption is semi-analytically derived from ocean color data, this algorithm depends less on empirical relationships established for particular time periods and areas. Our pan-Arctic dataset and robust semi-analytical methods should improve satellite estimates of DOC concentrations in surface waters of the Arctic Ocean and help to enhance our understanding of modifications of DOC cycles in the Arctic Ocean. Further work regarding inter-annual variability in DOC budget is required.

We acknowledge that an issue regarding the seasonal variability in the relationship between DOC concentrations and CDOM absorption needs to be considered. While no study examining this issue has yet been conducted so far for Arctic waters, Mannino et al. [2008] demonstrated in the U.S. Middle Atlantic Bight that the intercept of the DOC versus $a_{CDOM}(443)$ relationship changed seasonally in their study region, whereas the slope remained unchanged. This result suggests that the effect of the intercept is important when estimating DOC concentrations from space and

Antonio 12/11/13 10:21 PM
Deleted: not

429 warrants further study.

430

431 **Acknowledgements**

432 We are grateful to the captain and crews of the Canadian Icebreaker *CCGS Amundsen*, *USCGC*
433 *Healy,* Japanese R/V *Mirai*, and R/V *Viktor Buynitsky*. Datasets from SBI2002 cruises were
434 provided by V. Hill on the basis of the applicable data policy
435 (http://www.eol.ucar.edu/projects/sbi/). Sampling for these cruises was supported by the Arctic
436 System Sciences program of the National Science Foundation OPP-0125049 and 0223375 and the
437 National Aeronautics and Space Administration (NASA) Sensor Intercomparison and Merger for
438 Biological and Interdisciplinary Studies (SIMBIOS) program NAG5-10528. Sampling for the
439 ICESCAPE cruises was supported by NASA grant NNX10AF42G to Kevin Arrigo. ICESCAPE
440 data used here were supported by NASA as follows: PRR800 radiometer (NNX11AF64G to B. G.
441 Mitchell) and particle absorption (NNX10AG05G to R. Reynolds and D. Stramski).

442 Absorption data for ICESCAPE cruises were provided by R. Reynolds and D. Stramski. This
443 study was conducted as part of the MALINA Scientific Program funded by ANR (Agence
444 Nationale de la Recherche), INSU-CNRS (Institut National des Sciences de l'Univers – Centre
445 National de la Recherche Scientifique), CNES (Centre National d'Études Spatiales) and ESA
446 (European Space Agency). We also thank a joint contribution to the research programs of UMI
447 Takuvik, ArcticNet (Network Centres of Excellence of Canada) and the Canada Excellence
448 Research Chair in Remote Sensing of Canada's New Arctic Frontier.

449

450 **Appendix A**

451 **A1. Comparison of chl *a* determination between HPLC and fluorometric method**

452 Chl *a* concentrations determined fluorometrically (chl a^{fluo}) were compared to those using the
453 HPLC (chl a^{HPLC}) technique (Figure A1). Correlation between the two quantities was high (r^2 =
454 0.89, N = 177), and slope was not significantly different from 1:1 line ($p < 0.0001$). This result

455 suggests that in this study, chl a^{fluo} can appropriately replace chl a^{HPLC} when chl a^{HPLC} is not
456 available.
457
458 **A2. Evaluation of estimated phytoplankton absorption using Bricaud and Stramski [1990]'s**
459 **method**
460 We evaluated the performance of the Bricaud and Stramski [1990]'s method to estimate
461 phytoplankton absorption using total particulate absorption data from the ICESCAPE1 cruise
462 (Figure A2). Results showed that $a_\varphi(\lambda)$ values can be derived with high accuracy using this method
463 at wavelengths in the visible spectral domain. This method was used for the NABOS dataset.
464
465 **A3. High UV absorption for some phytoplankton communities**
466 High in phytoplankton absorption spectra around 330 nm were observed at four stations during
467 ICESCAPE cruises. The presence of mycosporine-like amino acids (MAAs) in natural waters has
468 been reported at all latitudes [e.g., Karsten et al., 1991, 1998; Whitehead and Vernet, 2000; Tilstone
469 et al., 2010]. The majority of MAAs absorption peaks are observed at 330-334 nm due to several
470 types of MAAs (e.g., shinorine, Porphyra-334, Asterina; Carreto et al., 2005; Llewellyn and Airs,
471 2010]. A clear bump was also observed at 360 nm at station 38 during ICESCAPE1, which
472 corresponded to the peak of palythene [Llewellyn and Airs, 2010]. Although actual concentrations
473 of MAAs during our observations are not available, the strong UV absorption observed for some
474 samples in this study suggest MAAs were present. Since MAAs are water soluble, they may be
475 released from the cells upon freezing-melting processes of sea ice, senescence, or grazing entering
476 the dissolved organic pool and hence contribute to our $a_{CDOM}(443)$ estimates (circles in Figure 7). It
477 is interesting to note that $a_\varphi(\lambda)$ at 330 and 360 nm can influence $R_{rs}(\lambda)$ in the visible spectral
478 domain. A similar result was also observed using an empirical relationship between $a_{CDOM}(443)$ and
479 $K_d(380)/K_d(780)$ [Hooker, unpublished]. The strong impact of MAAs absorption and spectral
480 reflectance in the UV spectral domain during a massive red tide was reported by Kahru and

Mitchell.[1998] and is the basis for the Red Tide index published for the Global Imager (GLI) algorithm [Mitchell and Kahru, 2009]. This influence of MAAs on UV-Visible absorption may allow estimates of MAAs using ocean color data in the future if the challenge of atmospheric correction in the UV spectral domain can be solved.

References

Aas, E., Hokedai, J., Hojersley, N. K., Sandvik, R., and Sakshaug, E.: Spectral properties and UV-attenuation in Arctic Marine waters, in UV radiation and Arctic ecosystems, D. O. Hessen ed., Springer, Berlin, 2002.

Allali, K., Bricaud, A., and Claustre, H.: Spatial variations in the chlorophyll-specific absorption coefficients of phytoplankton and photosynthetically active pigments in the equatorial Pacific, J. Geophys. Res., 102, 12413-12423, 1997.

Amon, R. M. W., Rinehart, A. J., Duan, S., Louchouarn, P., Prokushkin, A., Guggenberger, G., Bauch, D., Stedmon, C., Raymond, P. A., Holmes, R. M., McClelland, J. W., Peterson, B. J., Walker, S. A., and Zhulidov, A. V.: Dissolved organic matter sources in large Arctic rivers, Geochim. Cosmochim. Acta, 94, 217-237, 2012.

Ardyna, M., Babin, M., Gosselin, M., Devred, E., Bélanger, S., Matsuoka, A., and Tremblay, J.-E.: Parameterization of vertical chlorophyll a in the Arctic Ocean: impact of the subsurface chlorophyll maximum on regional, seasonal and annual primary production estimates, Biogeosci., 10, 4383-4404, doi:10.5194/bg-10-43832013, 2013.

Arrigo, K. R., and van Dijken, G. L.: Secular trends in Arctic Ocean net primary production, J. Geophys. Res., 116, C09011, doi:10.1029/2011JC007151, 2011.

Arrigo, K. R., Hill, V., Bélanger, S., Hirawake, T., and Mitchell, G. B.: Estimates of net primary production from space-based measurements, in IOCCG report on polar seas, submitted.

Babin, M., Stramski, D., Ferrari, G. M., Claustre, H., Bricaud, A., Obolensky, G., and Hoepffner, N.: Variations in the light absorption coefficients of phytoplankton, nonalgal

particles, and dissolved organic matter in coastal waters around Europe, J. Geophys. Res., 108, doi:10.1029/2001JC00082, 2003.

Bélanger, S., Xie, H., Krotkov, N., Larouche, P., Vincent, W. F., and Babin, M.: Photomineralization of terrigenous dissolved organic matter in Arctic coastal waters from 1979 to 2003: Interannual variability and implications of climate change, Global Geochem. Cycles, 20, doi: 10.1029/2006GB002708, 2006.

Bélanger, S., Cizmeli, S. A., Ehn, J., Matsuoka, A., Doxaran, D., Hooker, S. B., and Babin M.: Light absorption and partitioning in Arctic Ocean surface waters: impact of multi year ice melting, Biogeosci., in press.

Benner, R., Louchouarn, P., and Amon, R. M. W.: Terrigenous dissolved organic matter in the Arctic Ocean and its transport to surface and deep waters of the North Atlantic, Global. Biogeochem. Cycles., 19, GB2025, doi:10.1029/2004GB002398, 2005.

Ben Mustapha, S., Bélanger, S., and Larouche, P.: Evaluation of ocean color algorithms in the southern Beaufort Sea, Canadian Arctic: New parameterization using SeaWiFS, MODIS, and MERIS spectral bands, Can. J. Remote Sens., 38, 1-22, 2012.

Bricaud, A., Morel, A., Babin, M., Allali, K., and Claustre, H.: Variations of light absorption by suspended particles with chlorophyll *a* concentration in oceanic (Case 1) waters: Analysis and implications for bio-optical models, J. Geophys. Res., 103, 31033-31044, 1998.

Bricaud, A. and Stramski, D.: Spectral absorption coefficients of living phytoplankton and nonalgal biogenous matter: a comparison between the Peru upwelling area and the Sargasso Sea, Limnol. Oceanogr., 35, 562-582, 1990.

Campbell, J. W.: The lognormal distribution as a model for bio-optical variability in the sea, J. Gephys. Res., 100, C7, 13237-13254, 1995.

Carreto, J. I., Carignan, M. O., and Montoya, N. G.: A high-resolution reverse-phase liquid chromatography method for the analysis of mycosporine-like amino acids (MAAs) in marine organisms, Mar. Biol., 146, 237-252, doi:10.1007/s00227-004-1447-y, 2005.

533 Cleveland, J. S., and Weidemann, A. D.: Quantifying absorption by aquatic particles: A multiple
534 scattering correction for glass-fiber filters, Limnol. Oceanogr., 38, 1321-1327, 1993.
535 Comiso, J. C., Parkinson, C. L., Gersten, R., and Stock, L.: Accelerated decline in the Arctic sea ice
536 cover, Geophys. Res. Lettr., 35, L01703, doi:10.1029/2007GL031972, 2008.
537 Doxaran, D., Ehn, J., Bélanger, S., Matsuoka, A., Hooker, S. B., and Babin, M.: Optical
538 characterization of suspended particles in the Mackenzie River plume (Canadian Arctic
539 Ocean) and implications for ocean colour remote sensing, Biogeosci., 9, doi:10.5194/bg-9-
540 3213-2012, 2012.
541 Fichot, C. G., and Benner, R.: A novel method to estimate DOC cocentrations from CDOM
542 absorption coefficients in coastal waters, Geophy. Res. Lettr., 38, L03610,
543 doi:10.1029/2010GL046152, 2011.
544 Frey, K. E., and Smith, L. C.: Amplified carbon release from vast West Siberian peatlands by 2100,
545 Geophys. Res. Lettr., 32, L09401, doi;10.1029/2004GL022025, 2005.
546 Garver, S. A., and Siegel, D. A.: Inherent optical property inversion of ocean color spectra and its
547 biogeochemical interpretation, Time series from the Sargasso Sea, J. Geophys. Res., 102,
548 C8, 18607-18625, 1997.
549 Heim, B., Abramova, E., Doerffer, R., Gunther, F., Holemann, J., Kraberg, R., Lantuit, H.,
550 Loginova, L., Martynov, F., Overduin, P. P., and Wegner, C.: Ocean colour remote sensing
551 in the Southern Laptev Sea: evaluation and applications, Biogeosci. Discuss., 10, 3849-
552 3889, 2013.
553 Hodgkins, R., Cooper, R., Wadham, J., and Tranter, M.: Suspended sediment fluxes in a high-
554 Arctic glacierised catchment: implications for fluvial sediment storage, Sediment Geology,
555 162, 105-117, 2003.
556 Holm-Hansen, O., Lorenzen, C. J., Holms, R. W., and Strickland, J. D. H.: Fluorometric
557 Determination of Chlorophyll, J. Cons. perm. int. Explor. Mer., 30, 3-15, 1965.
558 Hooker, S. B., Morrow J. H., and Matsuoka A.: The 1 % and 1 cm perspective in validationg and

559 deriving AOP data products, Biogeosci., 10, 4511-4527, doi:10.5194/bg-10-4511-2013,
560 2013.
561 ICES, Chemical measurements in the Baltic Sea: Guidelines on quality assurance. International
562 Council for the Exploration of the Sea, ICES Techniques in Marine environmental sciences,
563 35, edited by E. Lysiak-Pastuszak and M. Krysell,
564 http://www.ices.dk/pubs/times/times35/TIMES35.pdf, 2004.
565 IOCCG, Remote sensing of ocean colour in coastal, and optically-complex, waters, in *Reports of*
566 *the International Ocean-Colour Coordinating Group*, no. 3, edited by S. Sathyendranath, pp.
567 140., Dartmouth, 2000.
568 Kahru, M. and Mitchell, B. G.: Spectral reflectance and absorption of a massive red tide off
569 Southern California. J. of Geophys. Res., 103(C10), 21601-21609, 1998.
570 Karentz, D., McEuen, F. S., Land, M. C., and Dunlap, W. C.: Survey of mycosporine-like amino
571 acids in Antarctic marine organisms: potential protection from ultraviolet exposure, Mar.
572 Biol., 108, 157-166, 1991.
573 Karsten, U., Sawall, T., Hanelt, D., Bischof, K., Figueroa, F. L., Flores-Moya, A., and Wiencke, C.:
574 An inventory of UV-absorbing mycosporine-like amino acids in macroalgae from polar to
575 warm-temperate regions, Botanica Marina, 41, 443-453, 1998.
576 Kishino, M., Takahashi M., Okami, N., and Ishimaru S.: Estimation of the Spectral Absorption
577 Coefficients of Phytoplankton the sea, Bull. Mar. Science., 37, 634-642, 1985.
578 Kwok R.: Near zero replenishment of the Arctic multiyear sea ice cover at the end of 2005 summer,
579 Geophys. Res. Lettr., 34, L05501, doi:10.1029/2006GL028737, 2007.
580 Llewellyn, C. A., and Airs, R. L.: Distribution an abundance of MAAs in 33 species of microalgae
581 across 13 classes, Mar. Drugs, 8, 1273-1291, doi:10.3390/md8041273, 2010.
582 Mannino, A., Russ, M. E., and Hooker, S. B.: Algorithm development and validation for satellite-
583 derived distributions of DOC and CDOM in the U.S. Middle Atlantic Bight, J. Geophys.
584 Res., 113, C07051, doi:10.1029/2007JC004493, 2008.

585 Maritorena, S., Siegel, D. A., and Peterson, A. R.: Optimization of a semianalytical ocean color
586 model for global-scale applications, Appl. Opt, 41, 2705-2714, 2002.
587 Matsuoka, A., Bricaud, A., Benner, R., Para, J., Sempere, R., Prieur, L., Bélanger, S., and Babin,
588 M.: Tracing the transport of colored dissolved organic matter in water masses of the
589 Southern Beaufort Sea: relationship with hydrographic characteristics, Biogeosci., 9, doi:
590 10.5194/bg-9-925-2012, 2012.
591 Matsuoka, A., Hill, V., Huot, Y., Bricaud, A., and Babin, M.: Seasonal variability in the light
592 absorption properties of western Arctic waters: parameterization of the individual
593 components of absorption for ocean color applications, J. Geophys. Res., 116,
594 doi:10.1029/2009JC005594, 2011.
595 Matsuoka, A., Larouche, P., Poulin, M., Vincent, W., and Hattori, H.: Phytoplankton community
596 adaptation to changing light levels in the southern Beaufort Sea, Canadian Arctic, Estuar.
597 Coast. Shelf Sci., 82, 537-546, 2009.
598 Matsuoka, A., Hooker, S. B., Bricaud, A., Gentili, B., and Babin, M.: Estimating absorption
599 coefficients of colored dissolved organic matter (CDOM) using a semi-analytical algorithm
600 for southern Beaufort Sea waters: applications to deriving concentrations of dissolved
601 organic carbon from space, Biogensci., 10, doi: 10.5194/bg-10-917-2013, 2013.
602 Matsuoka, A., Huot, Y., Shimada, K., Saitoh, S., and Babin, M.: Bio-optical characteristics of the
603 Western Arctic Ocean: Implications for ocean color algorithms, Can. J. Remote Sen., 33,
604 503-518, 2007.
605 Mitchell, B. G. and Kiefer, D. A.: Chlorophyll *a* specific absorption and fluorescence excitation
606 spectra for light-limited phytoplankton. Deep-Sea Res. 1, 35(5), 639-663, 1988.
607 Mitchell, B. G.: Predictive bio-optical relationships for polar oceans and marginal ice zones, J. Mar.
608 Sys., 3, 91-105, 1992.
609 Mitchell, B. G., Kahru, M., Wieland, J., and Stramska, M.: Determination of spectral absorption
610 coefficients of particles, dissolved materials and phytoplankton for discrete water samples, in

Ocean Optics Protocols For Satellite Ocean Color Sensor Validation, Revision 4, Volume 4: Inherent optical properties: instruments, characterization, field measurements and data analysis protocols, NASA Tech. Rep., pp. 39-64, Greenbelt, Maryland, 2003.

Mitchell, B. G., and Holm-Hansen, O: Bio-optical properties of Antarctic Peninsula waters: differentiation from temperate ocean models, *Deep-Sea Research*, Vol. 38, No. 8-9A, pp. 1009-1028, 1991.

Mitchell, B. G. & Kahru, M. Bio-optical algorithms for ADEOS-2 GLI. J.Remote Sens. Soc.of Japan, 29(1), 80-85, 2009.

Morrow, J. H., S. B. Hooker, C. R. Booth, G. Bernhard, R. N. Lind, and J. W. Brown (2010), Advances in Measuring the Apparent Optical Properties (AOPs) of Optically Complex Waters. NASA Tech. Memo. 2010-215856, NASA Goddard Space Flight Center, Greenbelt, Maryland, 42-50pp.

Mueller, J.L., and Austin, R.W.: Ocean Optics Protocols for SeaWiFS Validation, Revision 1. NASA Tech. Memo. 104566, Vol. 25, S. B. Hooker, E. R. Firestone and J. G. Acker, Eds., NASA GSFC, Greenbelt, Maryland, 67 pp, 1995.

Orek, H., Doerffer, R., Rottgers, R., Boersma, M., and Wiltshire, K. H.: A bio-optical model for remote sensing of Lena water, Biogeosci. Discuss., 10, 4888-4925, 2013.

Pegau, S., Zaneveld, J. R., and Mueller, J. L.: Beam transmission and attenuation coefficients: instruments, characterization, field measurements, and data analysis, in Ocean optics protocols for satellite ocean color sensor validation, Revision 4, NASA Tech. Memo. Volume 4, J. L. Mueller, S. Giulietta, S. Fargion, C. R. McClain, Eds., NASA GSFC, Greenbelt, Maryland, 76 pp, 2003.

Raymond, P.A., McClelland, J. W., Holmes, R. M., Zhulidov, A. V., Mull, K., Peterson, B. J., Striegl, R. G., Aiken, G. R., and Gurtovaya, T. Y.: Flux and age of dissolved organic carbon exported to the Arctic Ocean: A carbon isotopic study of the five largest arctic rivers, Global. Biogeochem. Cycles., 21, GB4011, doi:10.1029/2007GB002934, 2007.

637 Reynolds, R., Matsuoka, A., Hirawake, T., and Mitchell, G.: Ocean color algorithms and bio-optical
638 relationships for polar seas, IOCCG on polar seas, submitted.
639 Rottgers, R., and Gehnke, S.: Measurement of light absorption by aquatic particles: improvement of
640 the quantitative filter technique by use of an integrating sphere approach, Appl. Opt., 51,
641 1336-1351, 2012.
642 Shiklomanov, I. A.: World fresh water resources, In *Water in Crisis: A guide to the world's Fresh*
643 *Water Resources*, edited by P. H. Gleick, pp. 13-24, Oxford Univ. Press, New York, 1993.
644 Stroeve, J., Serreze, M., Drobot, S., Gearheard, S., Holland, M., Maslanik, J., Meier, W., and
645 Scambos, T.: Arctic sea ice extent plummets in 2007, EOS Trans., AGU, 89(2), 13-14, 2008.
646 Tassan, S., and Ferrari, G. M.: A sensitivity analysis of the 'Transmitance-Reflectance' method for
647 measuring high absorption by aquatic particles, J. Phyto. Res., 24, 757-774, 2002.
648 Tassan, S., and Ferrari, G. M.: An alternative approach to absorption measurements of aquatic
649 particles retained on filters, Limnol. Oceanogr., 40, 1358-1368, 1995.
650 Terrado, R., Lovejoy, C., Massana, R., and Vincent, W. F.: Microbial food web responces to light
651 and nutrients beneath the coastal Arctic Ocean sea ice during the winter-spring transition, *J.*
652 *Mar. Sys., 74*, 964-977, 2008.
653 Tilstone, G. H., Airs, R. L., Martinez-Vicente, V., Widdicombe, C., and Llewellyn, C.: High
654 concentrations of mycosporine-like amino acids and colored dissolved organic matter in the
655 sea surface microlayer off the Iberian Peninsula, Limnol. Oceanogr., 55(5), 1835-1850, 2010.
656 Twardowski, M. S., Boss, E., Sullivan, J. M., and Donaghay, P. L.: Modeling the spectral shape of
657 absorption by chromophoric dissolved organic matter, Mar. Chem., 89, 69-88, 2004.
658 Stedmon, C. A., Amon, R. M. W., Rinehart, A. J., and Walker, S. A.: The supply and characteristics
659 of colored dissolved organic matter (CDOM) in the Arctic Ocean: Pan Arctic trends and
660 differences, Mar. Chem., 124, 108-118, 2011.
661 Suzuki, R., and Ishimaru, T.: An improved method for the determination of phytoplankton
662 chlorophyll using n,n-dimethylformamide, J. Oceanogr., 46, 190-194, 1990.
663 Walker, S., Amon, R. M. W., and Stedmon, C. A., Variations in high latitude chromophoric

dissolved organic matter: a comparison of large arctic rivers, in press.

Wang, J., Cota, G. and Ruble, D. A.: Absorption and backscattering in the Beaufort and Chukchi Seas, J. Geophys. Res., 110(C4), C04014, 2005.

Wheeler, P. A., Gosselin, M., Sherr, E., Thibault, D., Kirchman, D. L., Benner, R., and Whiteledge, T. E.: Active cycling of organic carbon in the central Arctic Ocean, *Nature, 380*, 697-699, 1996.

Whitehead, K., and Vernet, M.: Influence of mycosporine-like amino acids (MAAs) on UV absorption by particulate and dissolved organic matter in La Jolla Bay, Limnol. Oceanogr., 45(8), 1788-1796, 2000.

673 **Figure captions**

674 Figure 1. Locations of sampling stations for the SBI spr (green circles), SBI sum (green diamonds),
675 CASES (blue circles), MR aut (brown circles), NABOS (purple circles), MALINA (red
676 circles), ICESCAPE1 (gold circles), and ICESCAPE2 (gold diamonds) in the Arctic Ocean.

677 Figure 2. Histogram of the total non-water absorption at 443 nm ($a_{tw}(443)$, m^{-1}) for SBI spr, SBI
678 sum, MR (left) and CASES, NABOS, MALINA (right).

679 Figure 3. Histogram of CDOM absorption at 443 nm ($a_{CDOM}(443)$, m^{-1}) for SBI spr, SBI sum, MR
680 (left) and CASES, NABOS, MALINA (right).

681 Figure 4. The contribution of absorption coefficients of phytoplankton ($a_{\varphi}(443)$, m^{-1}), NAP
682 ($a_{NAP}(443)$, m^{-1}), and CDOM ($a_{CDOM}(443)$, m^{-1}) absorption coefficients to the total non-
683 water absorption at 443 nm. See Figure 1 for symbols.

684 Figure 5. (a) Relationship between the total particulate absorption coefficients at 443 nm ($a_p(443)$,
685 m^{-1}) and chl *a* for our Arctic datasets. The regression line ($a_p(443) = 0.0548[\text{chl } a]^{0.658}$, N =
686 657; $p < 0.0001$) and +- 95 % confidence intervals are displayed. The regression line
687 obtained by Bricaud et al. [1998] (grey) is also overlaid for comparison. (b) Relationship
688 between $a_{\varphi}(443)$ and chl *a* ($a_{\varphi}(443) = 0.0315[\text{chl } a]^{0.733}$, $N = 657$; $p < 0.0001$).

689 Figure 6. Relationship between $a_{\varphi}(443)$ and $a_{\varphi}(\lambda)$ at 412, 490, 555, and 670 nm. Coefficients of
690 determination are shown in Table 3.

691 Figure 7. A comparison of estimated CDOM absorption ($a_{CDOM}^{mod}(443)$, m^{-1}) and *in situ*
692 measurements ($a_{CDOM}^{obs}(443)$, m^{-1}) using datasets (MALINA, ICESCAPE1, and
693 ICESCAPE2) that were not used for developing our CDOM algorithm (i.e., data from SBI
694 spr, SBI sum, and MR cruises were used for the algorithm development). Phytoplankton
695 absorption spectra for four data points above the 50 % error are shown and explained in
696 Figure A3 and Appendix A3.

697 Figure 8. Climatology of CDOM absorption at 443 nm from satellite sensors ($a_{CDOM}^{sat}(443)$, m^{-1})
698 from June to September, obtained by applying our CDOM absorption algorithm to MODIS

699 monthly-averaged climatology of $R_{rs}(\lambda)$ data over the 2002-2012 period. Three areas were
700 defined for examination of $a_{CDOM}^{sat}(443)$ values as follows: southern Beaufort (SB: 125 –
701 145° W, 68 – 72° N), Laptev (LP: 100 – 145° E, 69 – 77° N), and Kara seas (KR: 50 – 100°
702 E, 64 – 77° N). Histograms of $a_{CDOM}^{sat}(443)$ values within these areas are shown in Figure 9.
703 Figure 9. Histogram of $a_{CDOM}^{sat}(443)$ values in the SB, the LP, and the KR seas defined in Figure 8.
704 Figure 10. *In situ* relationships between DOC and $a_{CDOM}(443)$ for WAO (M12: Matsuoka et al.,
705 2012; $r^2 = 0.97$, $p < 0.0001$; $DOC = 55 + 357*a_{CDOM}(443)$) and EAO (W13: Walker et al., in
706 press; $r^2 = 0.90$, $p < 0.0001$; $DOC = 245 + 171*a_{CDOM}(443)$). The ranges of $a_{CDOM}(443)$ and
707 DOC concentrations for the regressions provided by M12 and Walker et al. [in press] and
708 applied in this study were as follows: $0.018\ m^{-1} < a_{CDOM}(443) < 1.08\ m^{-1}$; $55\ \mu M < DOC <$
709 $500\ \mu M$, $0.39 < a_{CDOM}(443) < 7.9\ m^{-1}$; $166 < DOC < 1660\ \mu g\ L^{-1}$).
710 Figure 11. Climatology of DOC concentrations in Arctic coastal waters (DOC^{sat}) from June to
711 September, obtained by applying the DOC versus $a_{CDOM}(443)$ regressions to the
712 $a_{CDOM}^{sat}(443)$ images shown in Figure 8. For WAO, the regression obtained by Matsuoka et
713 al.[2012] was applied within the measured range of $a_{CDOM}(443)$ (i.e., $0.018 < a_{CDOM}(443) <$
714 $1.08\ m^{-1}$). For EAO, the regression obtained Walker et al. [in press] was applied within the
715 measured range of $a_{CDOM}(443)$ (i.e., $0.018 < a_{CDOM}(443) < 8.1\ m^{-1}$). To obtain those values,
716 $a_{CDOM}(443)$ was estimated from $a_{CDOM}(350)$ by assuming $S_{CDOM} = 0.0175\ nm^{-1}$ for EAO
717 [Aas et al., 2002; Stedmon et al., 2011]. Histograms of DOC^{sat} values within the white boxes
718 defined in Figure 8 are shown in Figure 12.
719 Figure 12. Histogram of DOC^{sat} values in the SB, LP, and KR seas defined in Figure 8.
720 Figure A1. Comparison of chl *a* determined fluorometrically (chl a^{fluo}) with chl *a* using HPLC
721 method (chl a^{HPLC}).
722 Figure A2. Comparison of $a_\varphi(\lambda)$ estimated using Bricaud and Stramski [1990]'s method with *in situ*
723 measurements during the ICESCAPE1 cruise.
724 Figure A3. Spectra of phytoplankton absorption coefficients ($a_\varphi(\lambda)$, m^{-1}) at four stations during

ICESCAPE1&2 cruises. CDOM absorption estimates at these points were outside of 50 % errors as shown in Figure 7.

Table 1. Summary of our absorption datasets. The total non-water absorption ($a_{tw}(\lambda)$, m^{-1}), and individual contribution by phytoplankton ($a_{\varphi}(\lambda)$, m^{-1}), NAP ($a_{NAP}(\lambda)$, m^{-1}), and CDOM ($a_{CDOM}(\lambda)$, m^{-1}) are shown. To obtain $a_{\varphi}(\lambda)$ and $a_{NAP}(\lambda)$ values, a different β-factor was used for each instrument because of the different geometry and phytoplankton species composition (see below).

Year	Season	Cruise	$a_{tw}(443)$	$\%a_{\varphi}(443)$	$\%a_{NAP}(443)$	$\%a_{CDOM}(443)$	N	β-factor
2002	Spring	SBI spr	0.10 ± 0.04	0.27 ± 0.15	0.15 ± 0.10	0.58 ± 0.20	68	1
2002	Summer	SBI sum	0.11 ± 0.13	0.31 ± 0.14	0.16 ± 0.10	0.53 ± 0.16	107	1
2003-2004	Spring/Summer/Autumn	CASES	0.19 ± 0.20	0.16 ± 0.15	0.15 ± 0.10	0.68 ± 0.18	112	2*
2004	Autumn	MR	0.10 ± 0.06	0.18 ± 0.12	0.08 ± 0.05	0.74 ± 0.14	179	1
2007	Summer	NABOS	0.32 ± 0.15	0.08 ± 0.04	0.08 ± 0.04	0.85 ± 0.07	18	3*
2009	Summer	MALINA	0.19 ± 0.45	0.13 ± 0.09	0.15 ± 0.15	0.73 ± 0.18	119	4§
Average	All	All	0.14 ± 0.23	0.20 ± 0.14	0.13 ± 0.11	0.68 ± 0.19	603	-

1: Cleveland and Weidemann. [1993]

2: Tassan and Ferrari. [1995, 2002]

3: Bricaud and Stramski. [1990]; Allali et al. [1997]

4: Bélanger et al. [in press]

*Different β-factor was used for CASES [Tassan and Ferrari, 2002] and NABOS [Bricaud and Stramski, 1990; Allali et al., 1997] using the same Perkin-Elmer 19 spectrophotometer equipped with a 60-mm integrating sphere. During NABOS cruise (late summer to autumn), a mean value of chl *b* to chl *a* ratio of 0.15 was observed, which was similar to that obtained in the southern Beaufort Sea over the same time period (0.19) when mixture of small phytoplankton (e.g., flagellates) dominated [Matsuoka et al., 2009]. This result suggests that small phytoplankton dominated in EAO waters during NABOS cruise. Bricaud and Stramski. [1990] and Allali et al. [1997] obtained a β-factor for smaller type of phytoplankton species, which was applied for the NABOS dataset. For the CASES cruise, large phytoplankton such as diatoms dominated [Terrado et al., 2008]. Tassan and Ferrari. [1995, 2002] determined a β-factor for larger phytoplankton, which was applied to the CASES dataset.

747 [§]A Perkin-Elmer 19 spectrophotometer equipped with a 150-mm integrating sphere was used.

748

749 Table 2. Average values and standard deviations of $a_{NAP}(443)$ normalized by SPM ($a_{NAP}(443)^*$, m^2

750 g^{-1}). *N* indicates the number of samples. For comparison, values obtained for the COASTLOOC

751 cruises in the literature [Babin et al., 2003] are also shown.

	Cruise	$a_{NAP}(443)^*$	*N*
This study	CASES	0.0360 ± 0.0275	107
	NABOS	0.0014 ± 0.0019	15
	MALINA	0.0602 ± 0.0300	121
	All	0.0459 ± 0.0324	243
	All but NABOS	0.0488 ± 0.0312	228
Babin et al. [2003]	COASTLOOC	0.0410 ± 0.0230	328

752

753

754 Table 3. Correlations between $a_\varphi(\lambda)$ and $a_\varphi(443)$ in this study.

$a_\varphi(\lambda)$ at wavelength	412	490	555	670	N
r^2	0.98	0.99	0.87	0.95	993

755
756
757

Table 4. Statistics of $a_{CDOM}(443)$ and $a_{NAP}(443)$ at 443 nm with their spectral slopes, S_{CDOM} and S_{NAP}, respectively.

Cruise	$a_{CDOM}(443)$ Geometric mean (SD)	S_{CDOM} Arithmetic mean ± 1 SD	$a_{NAP}(443)$ Geometric mean (SD)	S_{NAP} Arithmetic mean ± 1 SD	N
SBI spr	0.0534 (2.1231)	0.0184 ± 0.0036	0.0114 (2.4180)	0.0095 ± 0.0022	80
SBI sum	0.0429 (1.7890)	0.0205 ± 0.0035	0.0115 (2.7128)	0.0102 ± 0.0015	111
MR	0.0662 (1.6732)	0.0155 ± 0.0031	0.0062 (2.1135)	0.0108 ± 0.0009	179
CASES	0.0992 (2.6003)	0.0198 ± 0.0027	0.0187 (4.3476)	0.0103 ± 0.0011	132 (173)
NABOS	0.2463 (1.8366)	0.0209 ± 0.0044	0.0141 (2.7972)	0.0165 ± 0.0062	31 (22)
MALINA	0.0559 (2.1947)	0.0185 ± 0.0013	0.0078 (4.8963)	0.0070 ± 0.0014	326 (436)
All	0.0642 (2.2577)	0.0184 ± 0.0032	0.0095 (3.9657)	0.0090 ± 0.0026	859 (1001)

762 Table 5. Comparison of $a_{CDOM}(443)$ estimates ($a^{mod}_{CDOM}(443)$, m^{-1}) with *in situ* $a_{CDOM}(443)$
763 ($a^{obs}_{CDOM}(443)$, m^{-1}) using independent datasets which were not used for developing the CDOM
764 algorithm. Data from MALINA, ICESCAPE1, and ICESCAPE2 were used. Root mean square error
765 (RMSE) and mean normalized bias (MNB) as well as coefficient of determination (r^2), intercept,
766 and slope are provided.
767

Datasets	r^2	Intercept	Slope	RMSE	MNB	*N*
This study	0.87	-0.022	0.97	0.069	8.58	79

768
769

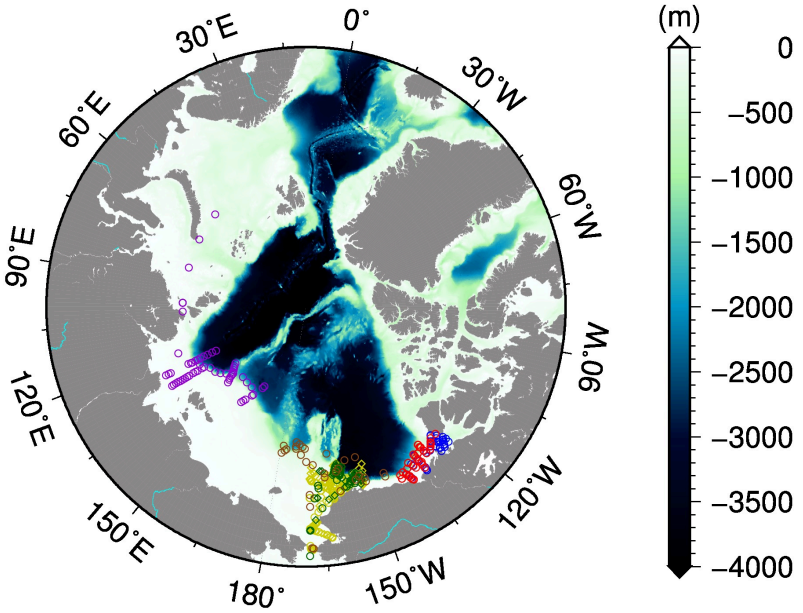

Figure 1

Matsuoka et al.

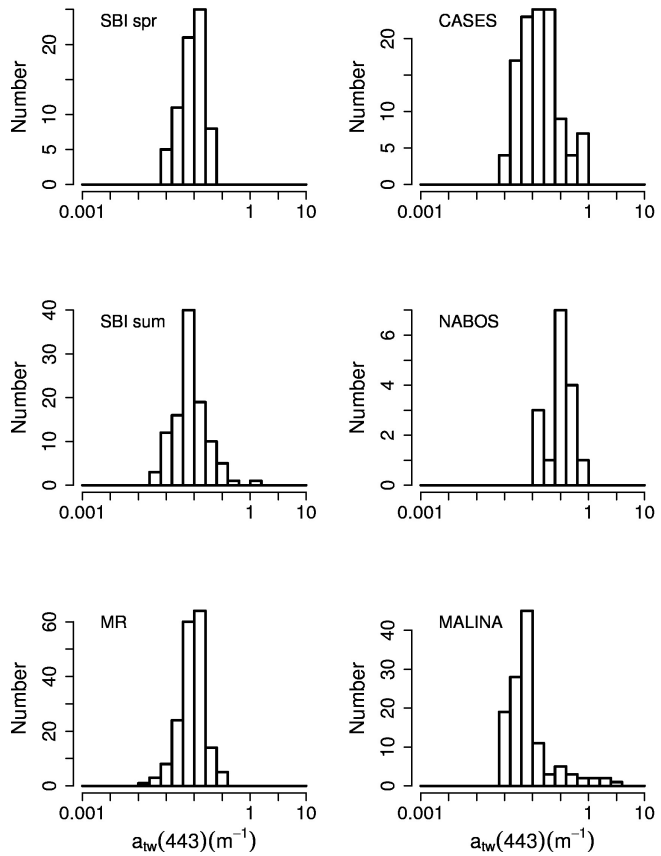

Figure 2

Matsuoka et al.

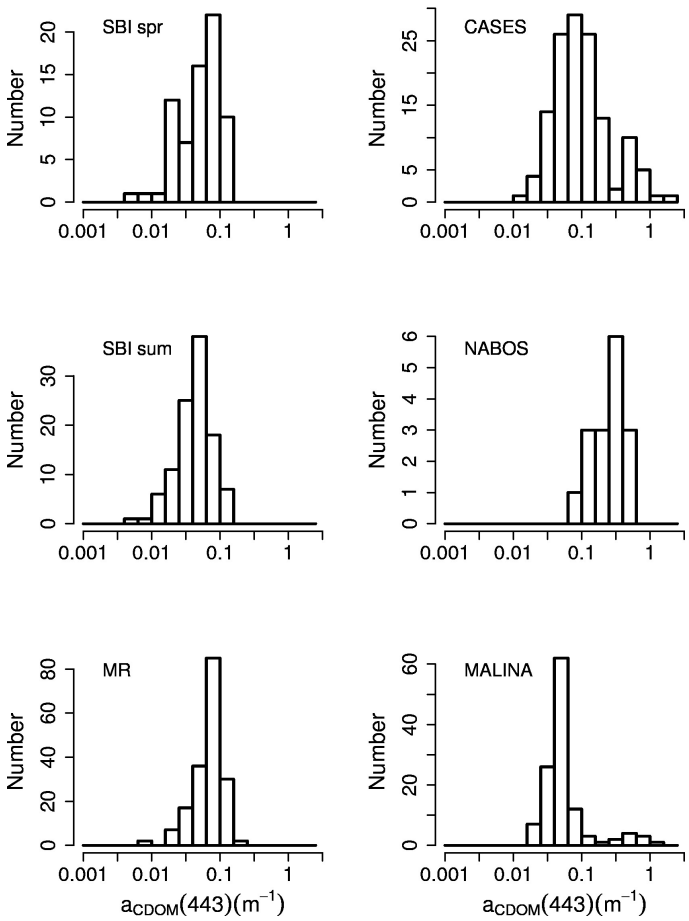

Figure 3

Matsuoka et al.

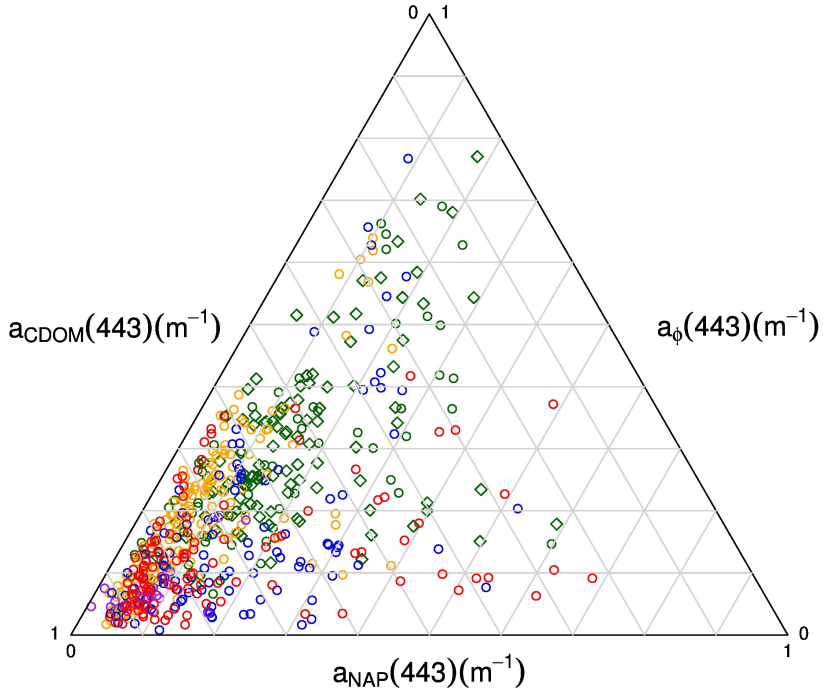

Figure 4

Matsuoka et al.

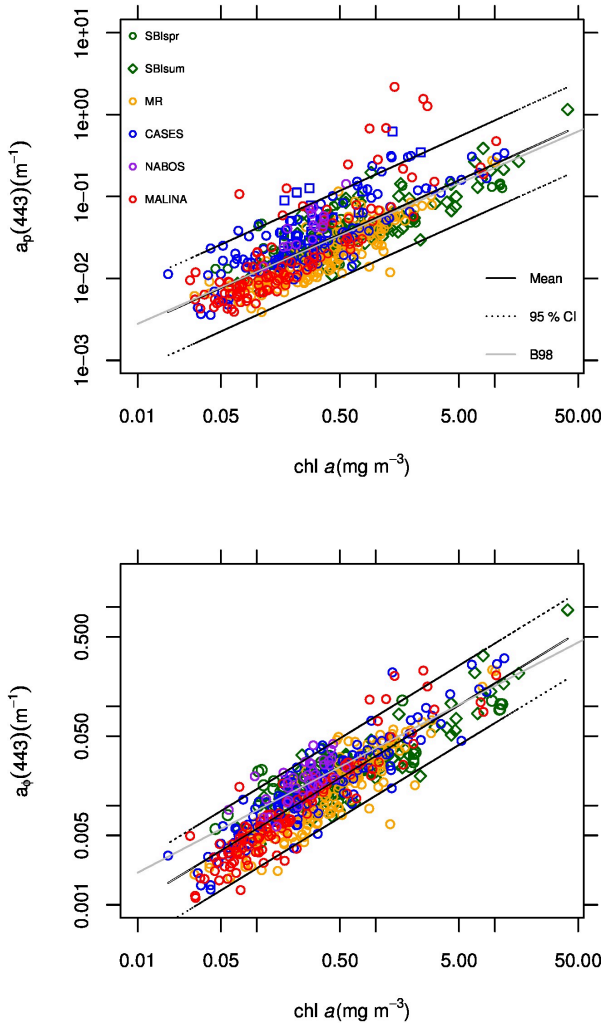

Figure 5

Matsuoka et al.

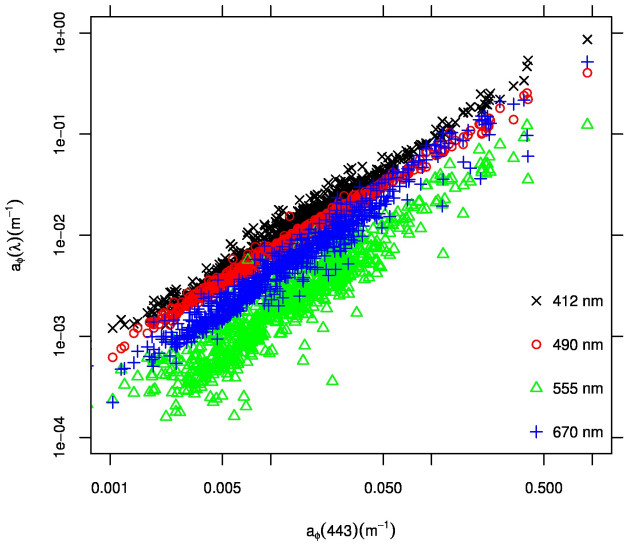

816

817

818

819

820

821

822

823

824

825

826

827 Figure 6

828 Matsuoka et al.

829

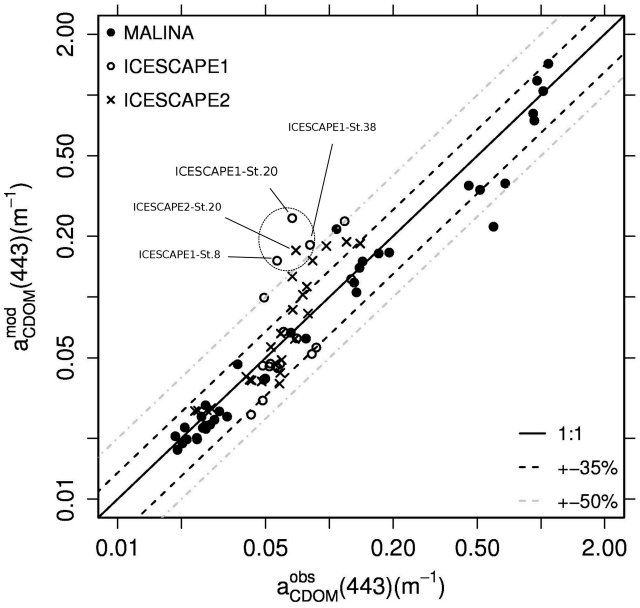

Figure 7

Matsuoka et al.

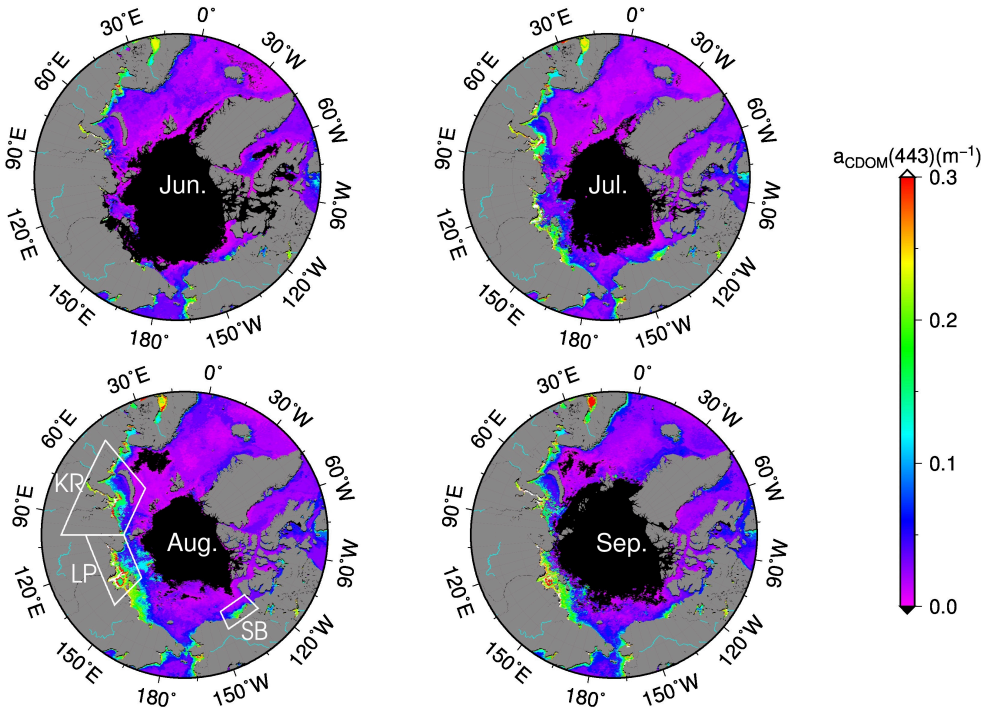

Figure 8

Matsuoka et al.

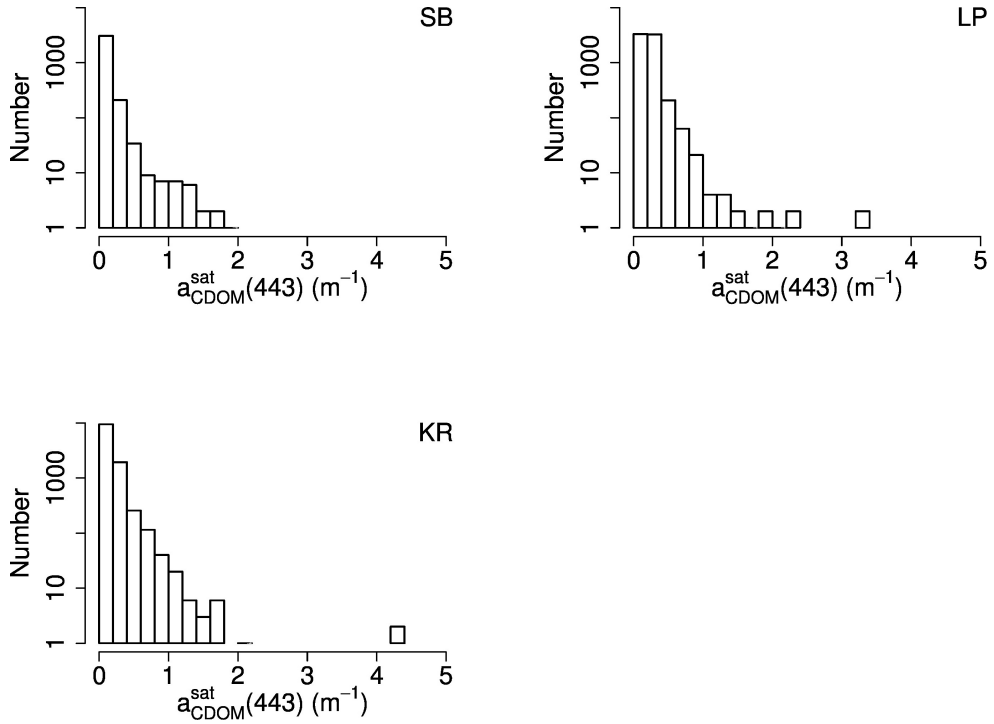

Figure 9

Matsuoka et al.

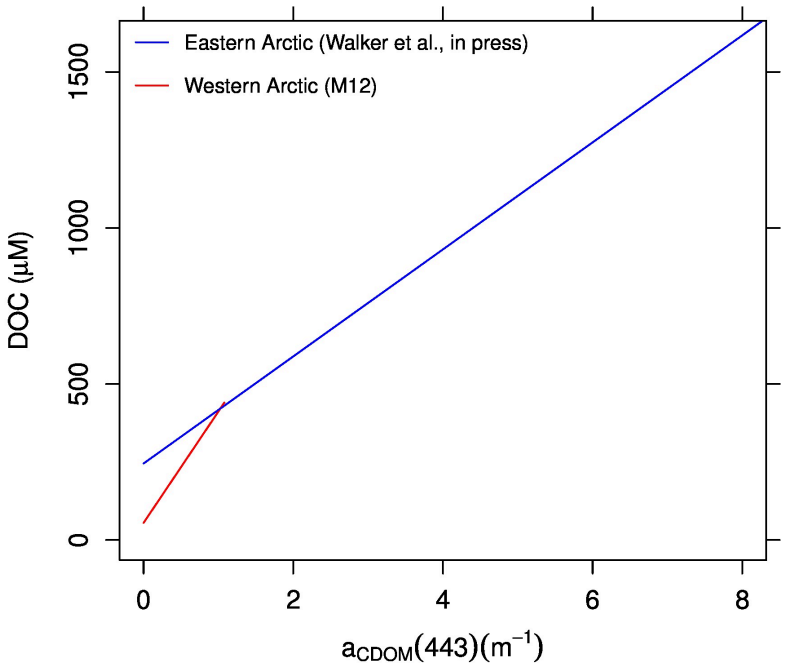

Figure 10

Matsuoka et al.

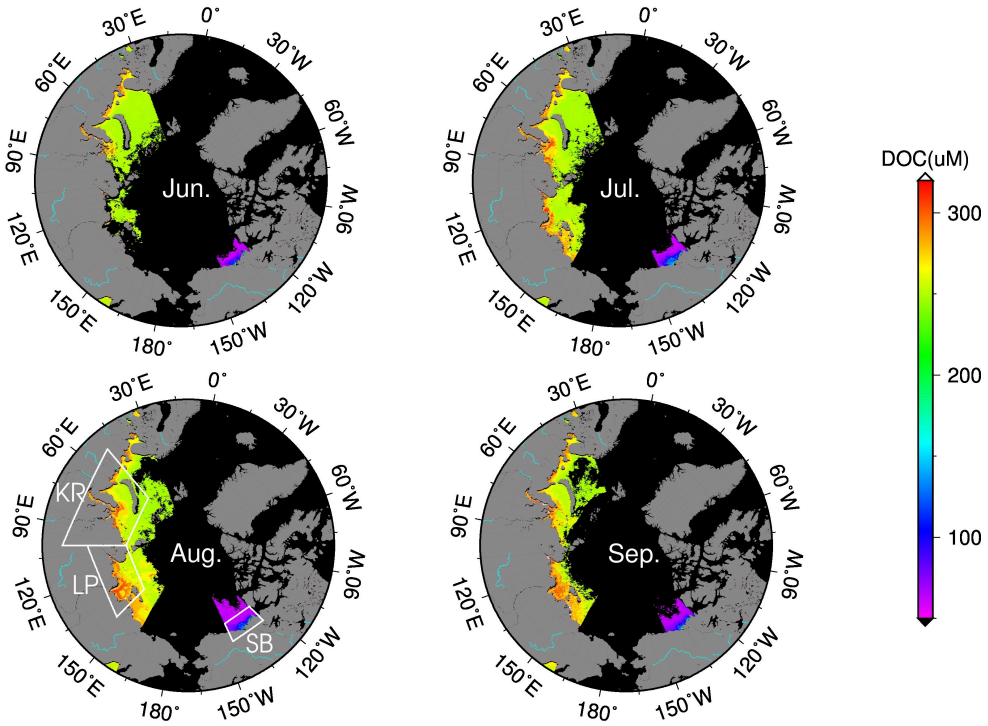

Figure 11

Matsuoka et al.

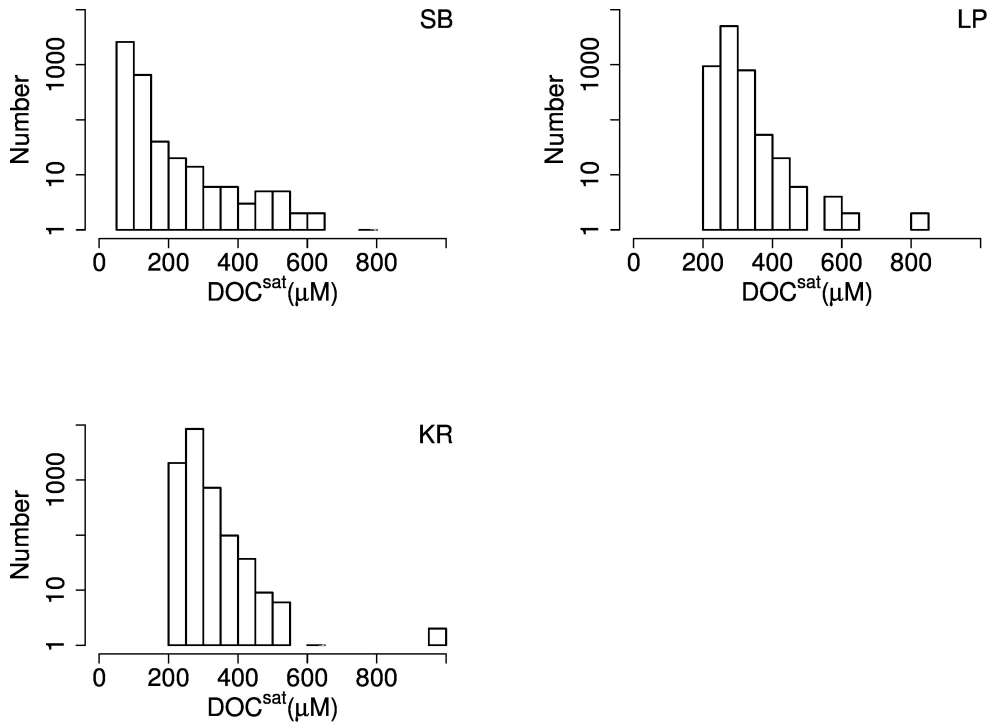

Figure 12

Matsuoka et al.

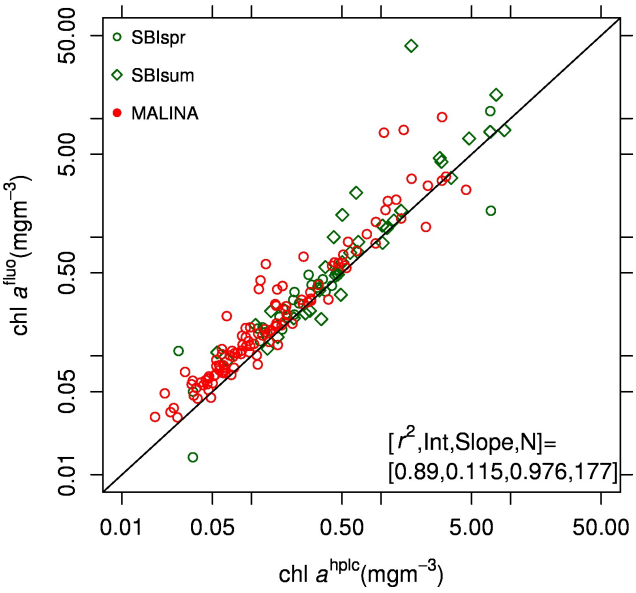

Figure A1

Matsuoka et al.

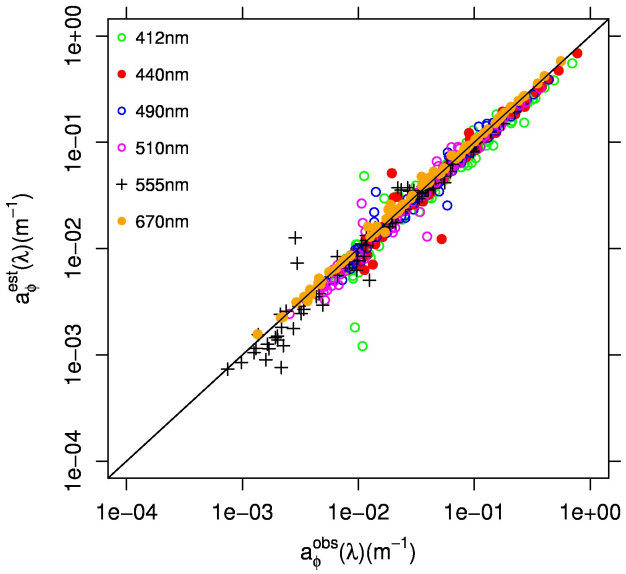

Figure A2

Matsuoka et al.

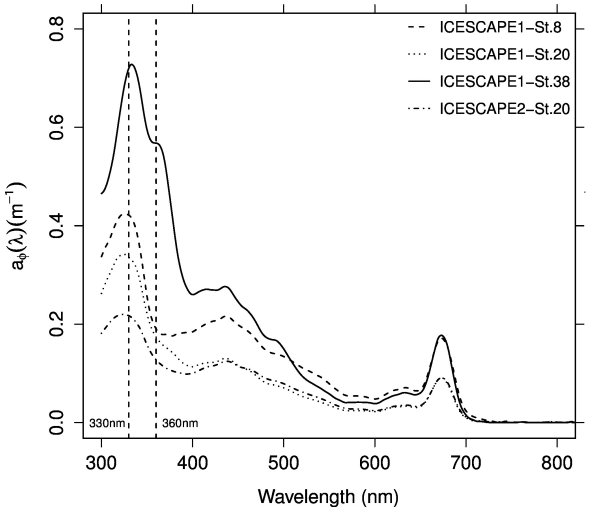

977

978

979

980

981

982

983

984

985

986

987 Figure A3

988 Matsuoka et al.

989

990